Ion energy measurements near a dormant cathode in a multiple-cathode gridded ion thruster

Joshua L. Rovey
Starfire Industries, Champaign, Illinois 61820

Alec D. Gallimore
University of Michigan, Ann Arbor, Michigan 48109

(Received 27 October 2006; accepted 15 January 2007; published online 14 March 2007)

A rectangular ion thruster discharge chamber was investigated for operation with multiple discharge cathode assemblies (DCAs). The multiple cathode approach attempts to increase thruster throughput and lifetime by operating three DCAs sequentially, possibly providing a threefold increase in discharge life. Previous multiple-cathode electric propulsion devices, such as the SPT-100, have shown dormant cathode erosion to be a life-limiting phenomenon. Similar results in a multiple-cathode discharge chamber may decrease the anticipated gain in discharge lifetime. In order to assess possible dormant cathode sputtering erosion, a diagnostic canister (DC) was designed and utilized to measure bombarding ion energy at the dormant cathode locations. The DC appeared similar to the active DCA, but was outfitted with a retarding potential analyzer. Most probable ion energy measurements show ions with energy of 27–35 eV (±10%) with respect to cathode common and ion energy increases with increasing magnetic field strength. These results are consistent with an ion falling from the plasma potential to cathode common. A simple sputtering erosion model shows that, if doubly charged ions are present, these energies are enough to cause sputtering erosion of the dormant units. © *2007 American Institute of Physics*. [DOI: 10.1063/1.2536514]

I. INTRODUCTION

Gridded ion thrusters are high-specific impulse, high-efficiency, advanced space propulsion systems. Three main processes compose gridded ion thruster operation: (i) electron generation; (ii) ion production through electron bombardment ionization; and (iii) ion extraction using high-voltage grids (ion optics). In modern ion thrusters, electrons are generated with a hollow cathode called the discharge cathode because it initiates and sustains the plasma discharge. Electrons from the cathode enter the discharge chamber and create ions through electron bombardment ionization collisions with neutral atoms, typically xenon. Plasma production is enhanced by increasing the electron path length with a magnetic field. Early gridded thrusters utilized divergent and radial magnetic field configurations, but modern thrusters utilize a ring-cusp geometry because it provides better plasma containment.[1] Ions are extracted and accelerated to significant velocity by high-voltage grids. One prominent example of a contemporary ring-cusp gridded ion thruster is the 30-cm-diam NASA Solar Technology and Application Readiness (NSTAR) ion thruster utilized on the Deep Space One (DS1) spacecraft.

Future deep-space missions will require an ion thruster that has long life and the ability to process a large quantity of propellant. In fact, an ion thruster may be required to operate continuously for as long as 14 years and process >2000 kg of propellant.[2–5] Results from the extended life test (ELT) of the flight spare DS1 NSTAR ion engine show that ion bombardment erosion of a molybdenum (Mo) keeper discharge cathode assembly (DCA) limits the operational lifetime of the ion thruster to ~30000 h.[6–8] Furthermore, wear test results for the NASA Evolutionary Xenon Thruster (NEXT) with a Mo keeper DCA show wear profiles similar to the NSTAR thruster,[9] suggesting it may also be limited in life due to ion bombardment erosion. Based on these results, one can conclude that contemporary ion thrusters utilizing a single, Mo keeper DCA are incapable of satisfying future mission requirements due to plasma ion bombardment of the DCA.[7]

Other DCA failure mechanisms can also occur after prolonged operation. Specifically, these include depletion of the barium in the insert, brought on by simple barium diffusion and subsequent evaporation, or the formation of tungstates that tie up the barium. Because of such phenomena, a single ion thruster hollow cathode may not be sufficient for missions requiring over 4 years of continuous thruster operation.[10]

One possible approach to increasing thruster throughput and operational lifetime is to use an ion thruster that sequentially operates mulitple DCAs. With this approach, a new DCA is ignited when the previous one fails. Ideally, a triple-DCA device will increase thruster discharge lifetime threefold, making longer mission times a possibility. The state-of-the-art in multiple cathode electric propulsion devices consists of two previous research endeavors: a double cathode ion thruster developed by Hughes Research Laboratories, and the Stationary Plasma Thruster, SPT-100.[11] In order to reduce the bombardment of high-energy ions on a single cathode operated at large discharge currents, the Hughes Research Laboratories developed a discharge chamber containing two hollow cathodes. Operation of the discharge chamber was accomplished with both cathodes operating together at multiple discharge conditions, including low-discharge-

current idling and operation with and without beam extraction. However, the cathodes were placed inside a plenum to facilitate uniform electron distribution, which caused significant increases in ion production cost. In fact, the plenum walls collected more ion current than was extracted in the ion beam.

Results from a 5700 h life test of the SPT-100 at the Jet Propulsion Laboratory showed that an operating cathode can cause significant erosion of the nonoperating cathode, thus reducing overall lifetime.[12–14] Specifically, propellant leaking through the inactive cathode created a "glow" discharge that produced enough ions to cause significant erosion of the dormant cathode. The unused cathode actually eroded at the higher rate. Eliminating the "glow" discharge may reduce the dormant cathode erosion, but results still indicate the inactive cathode collects an order of magnitude higher current density than the active cathode.[14]

Because of the results obtained during the SPT-100 life test, the possible erosion of a dormant cathode inside a multiple-cathode discharge chamber (MCDC) must be investigated. If the dormant cathodes inside an MCDC have reduced lifetimes due to pre-operation erosion, ion thruster lifetime and throughput may not increase as much as expected. With this in mind, a diagnostic canister (DC) that is similar in size and shape to the active DCA, but outfitted with a retarding potential analyzer (RPA), was used to measure ion energies near a MCDC dormant cathode. The following sections describe the experimental apparatus, data analysis procedure, results, lifetime implications, and conclusions.

II. EXPERIMENTAL APPARATUS AND SETUP

A. Vacuum facility

A large vacuum test facility (LVTF) was used for all experiments. The LVTF is a stainless-steel vacuum chamber with a diameter of 6 m and a length of 9 m. In order to reach high vacuum, the facility employs seven CVI TM-1200 reentrant cryopumps, each of which is surrounded by an LN_2 baffle. The cryopump system can be operated with any number of pumps in use. For the experiments described here, only two cryopumps were operated, which yielded a base pressure of 5.2×10^{-7} Torr. The chamber pressure was monitored using two hot-cathode ionization gauges, an external and a nude gauge. Pressure measurements from the gauges were corrected for xenon using the known base pressure on air and a correction factor of 2.87 for xenon as described in Ref. 15. Corrected operating pressures for all experiments reported here are below 4.2×10^{-6} Torr on xenon.

B. MCDC test article (TA)

The MCDC is a rectangular ion thruster discharge chamber based on the High-Power Electric Propulsion (HiPEP) thruster.[16] An electromagnet was placed on the backplate near the three DCA locations to adjust the magnetic field. A NEXT-type DCA was mounted to the backplate of the MCDC and utilized for all experiments. An ion collection grid was mounted at the ion extraction plane because the MCDC was operated as a simulated ion thruster without beam extraction.[17] Attachment of the ion collection grid, the electromagnet, and the NEXT DCA to the MCDC is referred to as the MCDC test article (TA), or simply TA. A schematic of the TA along with the chosen coordinate system is shown in Fig. 1.

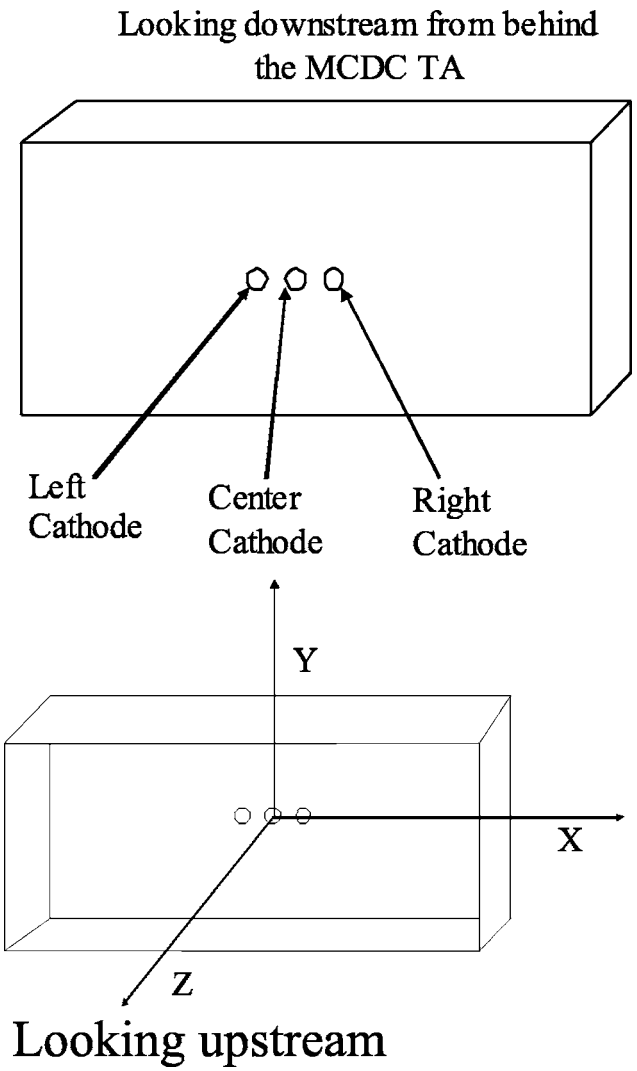

FIG. 1. MCDC coordinate system looking downstream (top) and looking upstream (bottom).

The general electrical setup of the TA was nearly identical to that described by Brophy,[17] however in this case an ion collection grid was utilized as the ion collection surface instead of high-voltage ion optics. The TA was operated with a 30 A discharge current, cathode common biased +25 V with respect to ground, and a collection grid bias of 20 V below cathode common. For the experiments presented here, ground refers to the vacuum facility potential and cathode common is the cathode potential.

For the experiments presented here, various electromagnet currents, DCA locations, and DC configurations were investigated. The DCA was operated at the left, center, and right locations for electromagnet currents of 0, +5, and +10 A. Furthermore, the RPA-DC was operated both electrically connected and electrically isolated (disconnected) from

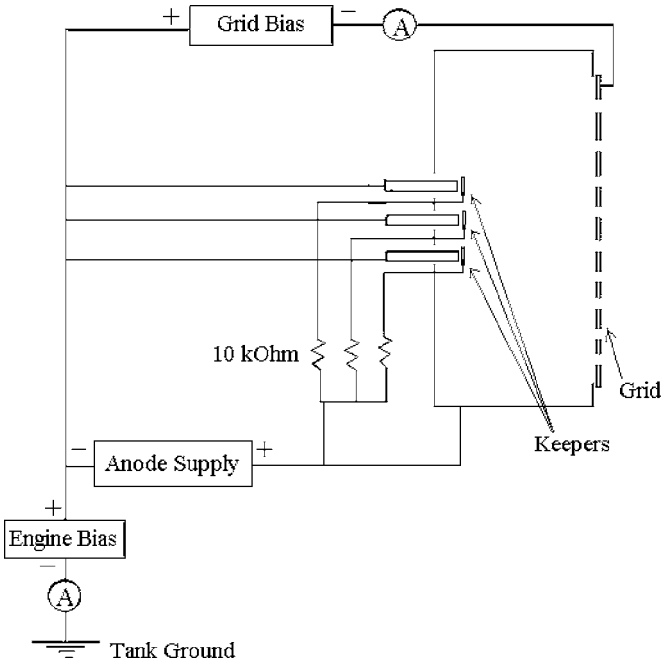

FIG. 2. Schematic of the MCDC TA electrical circuit.

the TA. A schematic of the electrical connections is shown in Fig. 2. More information regarding the RPA-DC and its operation is given in the following section. Further information regarding TA operation is described in Refs. 18 and 19.

C. Retarding potential analyzer (RPA) diagnostic canister (DC)

The retarding potential analyzer (RPA) DC appears similar in size and shape to the active DCA. However, the "cathode" tube has an internal miniature RPA. The miniature RPA was designed based on the multigridded energy analyzer described in Ref. 20, and the RPA described by Hofer,[21] Azziz,[22] and Beal.[23] Outer dimensions of the miniature RPA were approximately the same as the RPA described by Azziz,[22] which is approximately 50% smaller than that described by Hofer.[21]

The miniature RPA outer body was constructed of stainless steel with a diameter of 1.3 cm (0.50 in.) and had an entrance aperture identical to the active DCA orifice. Internal to the RPA were three grids, four ceramic spacers, and a collector. Each grid was stainless steel with a 0.13-mm thickness and 0.28-mm-diam holes arranged in a staggered pattern with a center-to-center spacing of 0.43 mm, yielding an open area fraction of 38%. The first grid was allowed to float to reduce the number density internal to the RPA. The second grid was biased 25 V below cathode common to repel electrons from reaching the collector. The potential of the third grid was swept from −25 to +45 V with respect to cathode common to repel ions. Finally, the collector was connected to ground through an ammeter to measure the collected current. Ceramic boron nitride spacers were used to electrically isolate the grids and collector. The electrical connectivity for each grid and the thickness of the spacers is described in Table I, which corresponds with Fig. 3.

TABLE I. RPA spacer dimensions and grid electrical bias setup.

Spacer	Thickness (mm)
1	3.4
2	3.4
3	1.0
4	1.0
Grid	**Potential w.r.t. cathode common (V)**
1	Float
2	−25
3	−25 to 45
4	Collector −25 V

The miniature RPA was placed inside a stainless-steel "keeper" tube and electrically isolated by another ceramic spacer. The body of the miniature RPA functions as the dormant "cathode" with the grids located internal to the "cathode." A photograph and schematic of the RPA-DC are shown in Figs. 3 and 4, respectively. Not shown in the photograph or the schematic are the two grids placed external to the RPA-DC covering the "keeper" orifice. These grids were required to reduce the plasma number density internal to the RPA. In order to function properly, the gap distance between grids 2 and 3 must be less than approximately four times the Debye length (λ_D) to avoid space-charge limitation of the grids.[20] Initial operation of the RPA was unsuccessful due to a large internal number density and hence a small Debye length. Adding grids external to the "keeper" was required to lower the RPA internal number density such that the Debye length met the required criteria. The external grids acted only to reduce the open area fraction of the "keeper" orifice and reduce the quantity of plasma present. Therefore, the energy distribution of ions entering the RPA through the grid-covered "keeper" orifice is assumed to be unaffected by the external grids.

The RPA-DC was utilized for left and middle DCA operation with TA electromagnet currents of 0, +5, and +10 A. Electrical connectivity of the DC was also investigated by either isolating the RPA-DC or connecting it to the TA. During electrically connected operation, the RPA body acted as the "cathode" and was connected to cathode common, while the "keeper" was connected to the anode through a 10 kΩ resistor.

The RPA-DC data acquisition setup was designed to measure the collector current as a function of the ion retarding grid potential. Collector current was monitored using a Keithley 486 picoammeter that was connected to ground. Data acquisition was controlled through a LabView interface that changed the source meter output voltage while recording the picoammeter current. Each sweep consisted of 1000 *I-V* pairs and required approximately 6 min. Averaging multiple sweeps was found to reduce the noise associated with data collection.

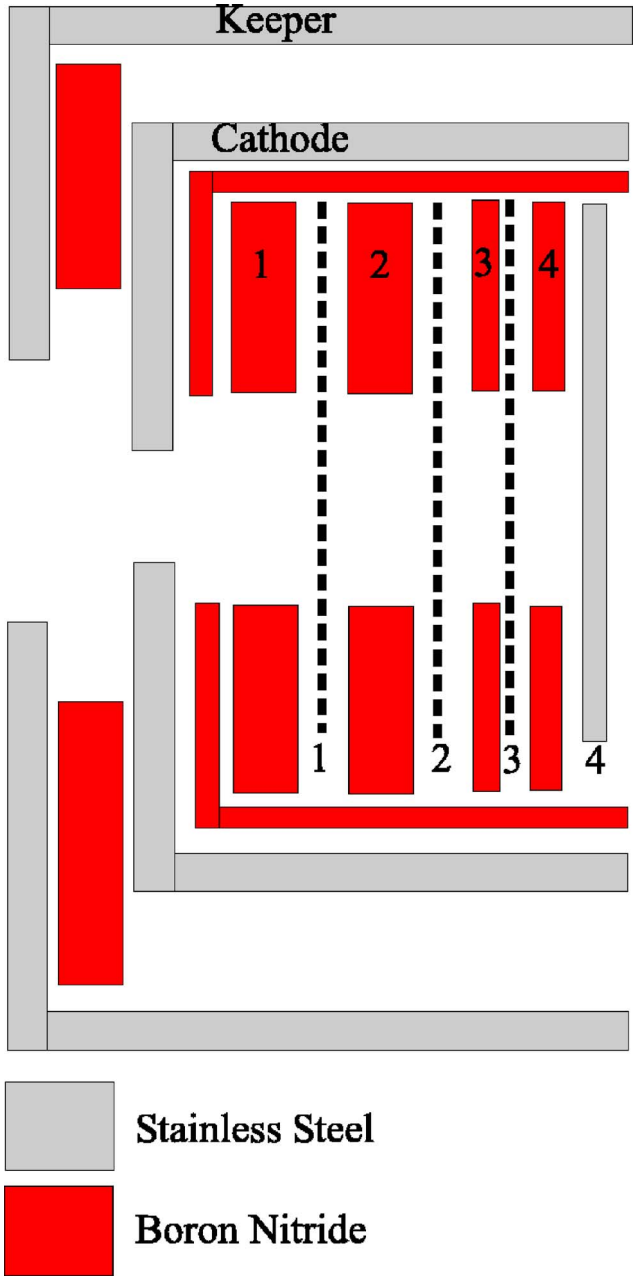

FIG. 3. (Color online) Schematic of the RPA-DC.

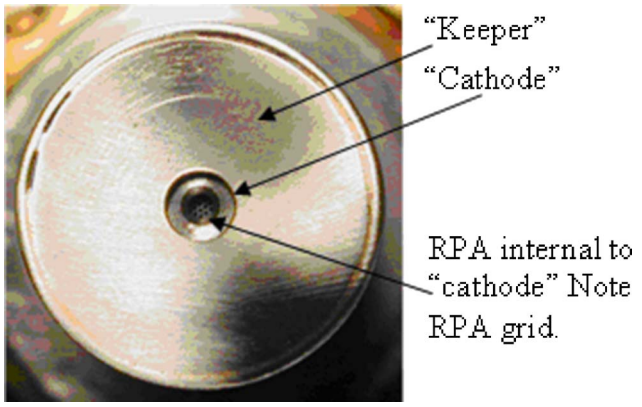

FIG. 4. (Color online) Photograph of the RPA-DC. Note the RPA grid internal to the "keeper" and "cathode."

III. RESULTS AND DISCUSSION

The experiment was designed to analyze the energy of ions bombarding the dormant cathodes. Specifically, bulk plasma ions that are near the dormant cathode and enter the RPA-DC orifice are analyzed by a RPA. As ions leave the bulk plasma and enter the RPA, they must first pass through a series of grids before being collected. Recording the collection electrode current as a function of retarding grid voltage yields the *I-V* characteristic. Ideally the ion energy distribution of bombarding ions would be experimentally measured. However, a RPA measures the energy distribution function only if the plasma is composed of ions of the same mass and charge. The charge states present in the TA plasma are currently unknown and multiply charged ions likely exist. Therefore, the RPA outputs the ion voltage distribution function because the energy-to-charge ratio of an ion is selectively filtered, not the energy [i.e., only ions with energy-to-charge ratios $V=E/(Z_i e)$ greater than the grid voltage pass and reach the collection electrode]. The ion voltage distribution function has the same reference as the retarding grid, i.e., cathode potential. Finally, the ion voltage distribution function is obtained by taking the derivative of the *I-V* characteristic, and this is illustrated in Eq. (1),[11,21]

$$\frac{dI}{dV} \propto f(V). \tag{1}$$

In this equation, I is the collection electrode current, V is retarding grid voltage, and $f(V)$ is the ion voltage distribution function. Of primary importance for the research presented here is the voltage value for the peak in the ion voltage distribution function, otherwise known as the most-probable voltage. This value is the ion energy per charge that is most likely obtained if an ion were randomly selected from the plasma near the dormant cathode. Because the voltage distribution function is measured with respect to the cathode potential, if the charge state of the impinging ion is known, its bombarding energy could be calculated by multiplying the charge state by this voltage.

Because the acquired raw data have enough noise to make the derivative meaningless, a certain amount of averaging, data interpolation, and smoothing were required. At least three data sweeps were acquired for each operational configuration and then averaged in order to reduce noise associated with these data. Then the data analysis routine was applied utilizing an IGOR 4.0 function that (i) interpolates, (ii) smooths, (iii) takes the derivative, and (iv) determines the most-probable voltage. Each interpolated *I-V* data pair was determined by linearly interpolating the preceding and following experimental data pair. Next, the interpolated data were smoothed utilizing a smoothing spline, which is a built-in IGOR function based on the algorithm described by Reinsche.[24] Next, the derivative of the smoothed data was taken to determine the ion voltage distribution function (the E/q distribution function). The last step in the RPA data analysis routine determined the most-probable voltage by lo-

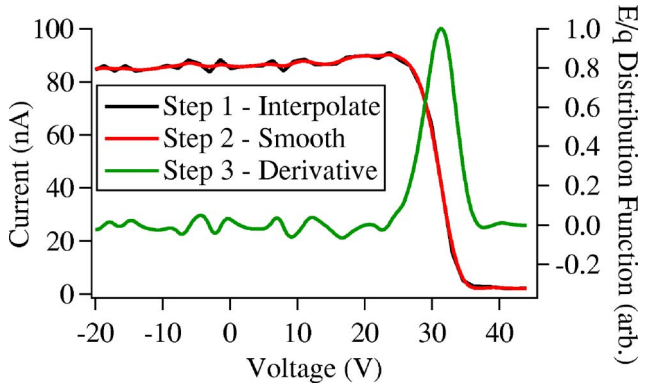

FIG. 5. (Color online) Example retarding potential analyzer (RPA) analysis routine results.

cating the voltage at which the peak in the distribution function occurs. A representative plot of the data throughout the analysis procedure is shown in Fig. 5.

The RPA-DC was utilized for left active and middle active DCA configurations. RPA-DC data were not obtained for the right active DCA configuration. A voltage sweep of 70 V was utilized because increasing the sweep to larger voltages did not reveal any interesting structures. The error associated with this method was estimated at 10% based on the repeatability of the measurements, the data analysis routine, and the error of the various hardware components utilized for data acquisition.

Figure 6 shows the peak E/q in the distribution function (most-probable voltage) as a function of the TA configuration. On the x axis are the 0, +5, and +10 A electromagnet current configurations. Data are presented for the middle (top) and left (bottom) active DCA configurations with the RPA-DC electrically connected or isolated from the TA. All voltages are referenced with respect to cathode common. Most-probable-voltage values range from 18 to 32 V above cathode common. Typical trends show the most-probable voltage (peak E/q) increasing with increasing electromagnet current. Furthermore, during middle DCA operation, the DC on the right side of the TA records a larger most-probable voltage. The middle DC records a larger most-probable voltage during left DCA operation. Operating the DCs electrically connected to or isolated from the TA does not affect the most-probable-voltage results. This result is expected because electron temperature and number density measurements inside the TA yield a Debye length of ~ 20 μm,[19] so changes in the dormant cathode potential do not propagate far into the bulk discharge plasma.

Measured most-probable voltages are typically larger than the discharge voltage ($\sim$24.5 V for the 0 A electromagnet configuration) and are similar to plasma potential measurements obtained in both the TA[19] and other ion thruster discharge chambers.[25] Results are consistent with ions falling from the plasma potential to reach the RPA collector. As electromagnet current increases, the axial magnetic field near the cathodes increases and the most-probable voltage increases. As the axial magnetic field increases, electrons emitted from the active DCA and created in the bulk discharge plasma are more confined to the field lines. Since fewer electrons are crossing field lines and getting close to the dormant cathodes, the plasma potential at those cathodes increases.

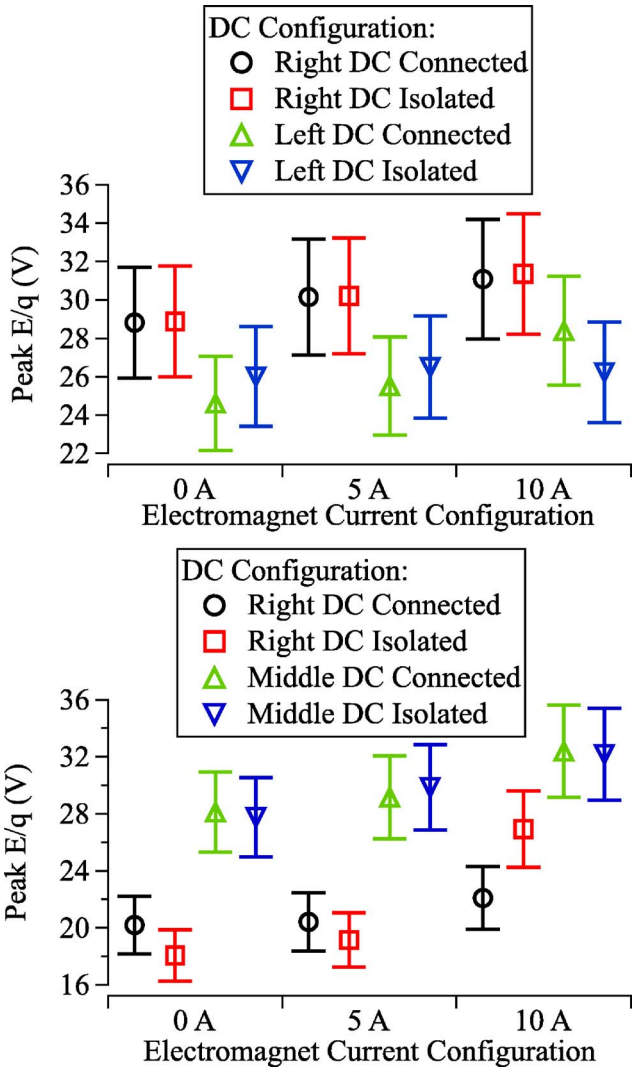

FIG. 6. (Color online) Peak E/q voltages (most-probable-voltage) obtained with the RPA-DC for the middle (top) and left (bottom) active DCA TA configurations.

Some of these results show voltages greater than or equal to 30 V, which is cause for concern, especially if there is a significant population of doubly charged ions present. Some of these ions can be expected to impact the dormant cathode and, if a significant doubly charged ion population exists, cause erosion of the dormant cathode. Doubly charged ions have been suggested as a dominant erosion-causing mechanism.[26]

IV. SPUTTERING EROSION IMPLICATIONS

In this section, the RPA most-probable-voltage results are utilized to predict the sputtering erosion of the dormant cathodes for both molybdenum (Mo) and carbon graphite keeper materials. Currently, most DCA keepers are constructed of Mo, but different materials with lower sputtering yields, such as graphite, are being investigated.[9] In order to predict the erosion of the dormant cathodes, an accurate sputtering yield model for low-energy xenon ions bombarding

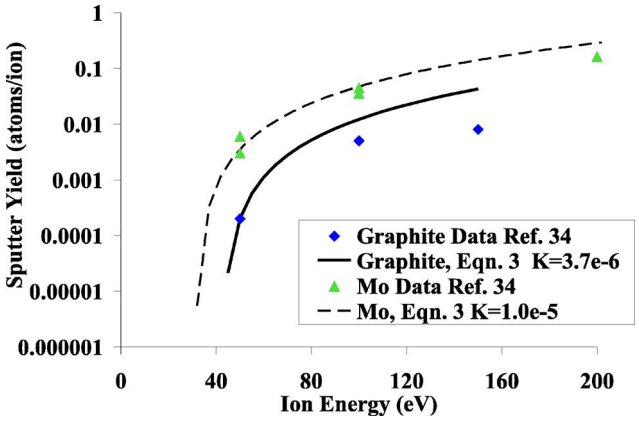

FIG. 7. (Color online) Equation (3) fit to Doerner *et al.*, molybdenum, and graphite sputter yield weight loss data for normal ion incidence (Ref. 34).

the keeper is required. Unfortunately, many models have been developed and no one model appears to be superior. Both Duchemin[27] and Nakles[28] have illustrated the uncertainty in sputtering yield and theory near threshold. For the analysis that follows, an erosion model is developed based on experimental data and sputtering theory. The output of the model is sputter yield as a function of bombarding ion angle of incidence.

Sputtering energy threshold as a function of incidence angle is assumed to be of the form described by Yamamura.[29] For small angles, the sputtering process dominates and Yamamura suggests the following relation:

$$E_{\text{th}}(\theta) = E_s[4.4 - 1.3\log(m_2/m_1)]\cos^2(\theta). \quad (2)$$

In this equation, E_s is sublimation energy (eV), m_1 and m_2 are the incident and target atom mass (kg/atom), respectively, and θ is the angle of incidence (degrees). The sublimation energy for Mo and graphite is 6.83 and 7.41 eV, respectively.[30,31] Herman[25] and Williams[32] suggest that ions bombarding the active DCA have presheath angles on the order of 60 deg, resulting in impacting angles of ~35 deg or less with respect to keeper normal. The impacting angle of ions bombarding the dormant cathodes is assumed to be equal to or less than that for the active DCA. Equation (2) is used to determine Mo and graphite sputtering threshold energy as a function of angle of incidence for angles less than 40 deg. Sputtering yields are calculated by adjusting the equation developed by Wilhelm[33] to account for both bombarding ion energy and incidence angle as illustrated in Eq. (3),

$$Y(E,\theta) = K[E - E_{\text{th}}(\theta)]^2. \quad (3)$$

In this equation, E is the bombarding ion energy (eV), E_{th} is the threshold energy for sputtering (eV), Y is the sputter yield (atoms/ion), and K is a constant. Doerner *et al.*[34] have measured sputter yields for normal incident xenon bombarding graphite and Mo using a weight-loss detection scheme. A curve fit of Eq. (3) assuming normal incident ions to the measured Mo and graphite sputter yield data is shown in Fig. 7. The fits yield K values of 3.7×10^{-6} and 1.0×10^{-5} for the graphite and Mo data, respectively. Each fit is made to have better agreement with the low-energy data because

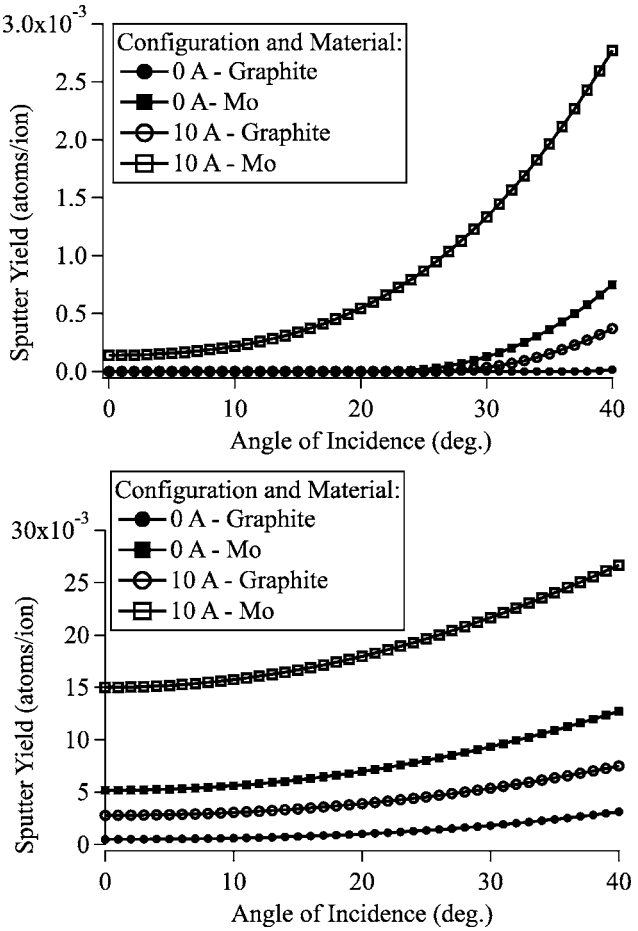

FIG. 8. Sputter yield as a function of angle of incidence for singly charged (top) and doubly charged (bottom) ions on a graphite or Mo dormant cathode keeper.

low-energy sputtering is of primary interest for this analysis.

Bombarding ion energy is calculated based on the RPA most-probable-voltage measurements. The most-probable voltages are assumed to be the plasma potential near the dormant cathodes. Initially stationary ions are assumed to fall through the potential difference between the plasma and keeper, as illustrated by Eq. (4). In this equation, V_p is the plasma potential and V_k is the keeper potential. Keeper potential is typically on the order of 4 V and is assumed constant for this analysis:

$$E = (V_p - V_k). \quad (4)$$

Results from the DCs suggest that for the two extreme operational configurations, 0 and +10 A electromagnet current, plasma potential values are 27 and 35 V, respectively, with respect to cathode common. These values are utilized in the model to calculate the sputter yield.

The predicted sputter yields for singly and doubly charged xenon ion bombardment on a Mo or graphite dormant cathode keeper in a MCDC are given in Fig. 8. As anticipated, singly charged xenon ions cause an order of magnitude less sputter erosion of the dormant cathode keeper because the bombarding ion energy is lower. As angle of incidence with respect to the keeper normal increases, the sputter yield increases. Because the 0 A electromagnet cur-

rent configuration has a lower plasma potential, ions gain less energy and the result is a lower sputter yield. In fact, an appreciable sputter yield is not calculated until the ion angle of incidence is approximately 25 degrees with respect to the keeper normal. The 10 A electromagnet current configuration has a larger plasma potential, so singly charged ions are capable of sputtering a Mo keeper. For a given electromagnet current configuration, the graphite keeper has a lower sputter yield, suggesting graphite may suffer less erosion than a Mo keeper dormant cathode.

Although the model presented provides insight into dormant cathode erosion, multiple approximations have been made. The following list describes and justifies some of the shortcomings of the erosion model: (i) Limited low-energy sputter data for graphite and molybdenum at normal and off-normal incidence are available, (ii) sputter threshold and yield data have large discrepancies (7–62 eV),[28] (iii) ion number density at the dormant cathode locations has been neglected, (iv) normal incidence sputter data are used for off-normal erosion predictions, and (v) ions in the high-energy tail of the distribution function have been neglected. As Fig. 7 shows, a slight increase in bombarding ion energy can cause significantly more erosion. Therefore, ions in the high-energy tail of the distribution function will cause more erosion than those at the most-probable voltage. However, it is likely that multiply charged ions exist in ion thruster discharge plasma and are causing the most erosion of the DCA.[25,26] Therefore, it is expected that multiply charged ions will also be the dominant erosion mechanism on the dormant cathodes. Future investigations will attempt to eliminate these approximations to better understand and predict dormant cathode erosion in a MCDC.

These erosion prediction results suggest graphite is the best choice to reduce dormant cathode keeper erosion. However, other phenomena may plague graphite keepers. Specifically, residual amounts of oxygen impurity ions may strike the surface along with the xenon plasma ions. The sputter yield of high-energy oxygen ions on carbon is orders of magnitude larger than low-energy xenon ion bombardment.[34] This effect must be better understood or eliminated, and further investigation into xenon-graphite sputtering behavior must be completed in order to validate graphite as an erosion-reducing, lifetime-increasing design solution.

V. CONCLUSIONS

Dormant cathode plasma properties were analyzed using a RPA-DC designed to appear similar to the active DCA. The DC was mounted at a dormant cathode location in a MCDC TA and operated over a variety of configurations. Most-probable-voltage (peak in the E/q distribution function) measurements were compared for the various configurations. Results show no noticeable difference between operating the DC electrically connected ("cathode" connected to cathode common and "keeper" connected to the anode through a 10 kΩ resistor) or electrically isolated (both "cathode" and "keeper" floating) from the TA. Most-probable-voltage values are consistent with previously measured plasma potential results, suggesting that any erosion-causing bombarding ions will be falling from the plasma potential. As the electromagnet current increases, the axial magnetic field increases, restricting electron access to the dormant cathodes. This causes the plasma potential near the dormant cathodes to increase.

Analysis of sputter erosion of the dormant cathodes due to singly and doubly charged xenon ion bombardment of a Mo or graphite keeper was presented utilizing a sputtering yield model. Results indicate that Mo dormant cathode keepers may erode significantly faster than graphite keepers, especially if doubly charged ions are present. This result suggests that graphite may be a better option for dormant cathode keeper material. However, other problems may plague graphite keepers, such as oxygen impurity ion bombardment.

ACKNOWLEDGMENTS

We would like to thank the entire research group at PEPL, who have been instrumental in this investigation, Jesse Linnell for assistance with the RPA setup and data acquisiton, Yassar Azziz for the miniature RPA drawings, and Terry Larrow for fabricating the hardware used in this study.

We would also like to thank Michael Patterson of NASA GRC for the financial support of this research through Research Grant No. NNC04GA67G and for use of government furnished equipment. We would like to acknowledge Dr. John Foster (grant monitor), who has been the principal contact at NASA GRC. J.L.R. was additionally supported through a Michigan Space Grant Consortium graduate fellowship. This support is gratefully acknowledged.

[1] J. S. Sovey, J. Spacecr. Rockets **21**, 488 (1984).
[2] M. J. Patterson, R. F. Roman, and J. E. Foster, *Ion Engine Development for Interstellar Precursor Missions* (American Institute of Aeronautics and Astronautics, Huntsville, AL, 2000), AIAA-2000-3811.
[3] S. Oleson, *Electric Propulsion Technology Development for the Jupiter Icy Moon Orbiter Project* (American Institute of Aeronautics and Astronautics, Fort Lauderdale, FL, 2004), AIAA-2004-3449.
[4] V. K. Rawlin, G. J. Williams, L. Pinero, and R. F. Roman, in *Proceedings, 27th International Electric Propulsion Conference* (Electric Rocket Propulsion Society, Pasadena, CA, 2001), IEPC-01-096.
[5] T. Randolph and J. E. Polk, *An Overview of the Nuclear Electric Xenon Ion System (NEXIS) Activity* (American Institute of Aeronautics and Astronautics, Fort Lauderdale, FL, 2004), AIAA-2004-3450.
[6] A. Sengupta, J. R. Brophy, J. R. Anderson, C. E. Garner, K. de Groh, T. Karniotis, and B. Banks, *An Overview of the Results from the 30,000 Hr Life Test of Deep Space 1 Flight Spare Ion Engine* (American Institute of Aeronautics and Astronautics, Fort Lauderdale, FL, 2004), AIAA-2004-3608.
[7] A. Sengupta, J. R. Brophy, and K. Goodfellow, *Status of the Extended Life Test of the Deep Space 1 Flight Spare Engine After 30,352 Hours of Operation* (American Institute of Aeronautics and Astronautics, Huntsville, AL, 2003), AIAA-2003-4558.
[8] A. Sengupta, in *Proceedings, 29th International Electric Propulsion Conference* (Electric Rocket Propulsion Society, Princeton, NJ, 2005), IEPC-2005-026.
[9] H. Kamhawi, G. C. Soulas, M. J. Patterson, and M. M. Frandina, *NEXT Ion Engine 2000 Hr Wear Test Plume and Erosion Results* (American Institute of Aeronautics and Astronautics, Fort Lauderdale, FL, 2004), AIAA-2004-3792.
[10] S. D. Kovaleski, M. J. Patterson, G. C. Soulas, and T. R. Verhey, in *Proceedings, 27th International Electric Propulsion Conference* (Electric Rocket Propulsion Society, Pasadena, CA, 2001), IEPC-01-271.
[11] L. B. King, Ph.D. thesis, University of Michigan (1998).
[12] C. E. Garner, J. R. Brophy, J. E. Polk, and L. C. Pless, *Cyclic Endurance Test of a SPT-100 Stationary Plasma Thruster* (American Institute of Aeronautics and Astronautics, Indianapolis, IN, 1994), AIAA-94-2856.

[13] C. E. Garner, J. R. Brophy, J. E. Polk, and L. C. Pless, *A 5,730 Hr Cyclic Endurance Test of the SPT-100* (American Institute of Aeronautics and Astronautics, San Diego, CA, 1995), AIAA-95-2667.
[14] M. Day, V. Kim, V. I. Kozlov, G. A. Popov, and A. I. Skrylnikov, *Investigation of the Nonoperating Cathode Erosion Reasons* (American Institute of Aeronautics and Astronautics, Lake Buena Vista, FL, 1996), AIAA-96-2710.
[15] S. Dushman, *Scientific Foundations of Vacuum Technique* (Wiley, New York, 1958), Vol. 4.
[16] J. E. Foster, T. W. Haag, H. Kamhawi, M. J. Patterson, S. Malone, F. Elliott, G. J. Williams, J. S. Sovey, and C. Carpenter, *The High Power Electric Propulsion Thruster* (American Institute of Aeronautics and Astronautics, Fort Lauderdale, FL, 2004), AIAA-2004-3812.
[17] J. R. Brophy, *Simulated Ion Thruster Operation Without Beam Extraction* (American Institute of Aeronautics and Astronautics, Orlando, FL, 1990), AIAA-90-2655.
[18] J. L. Rovey and A. D. Gallimore, J. Propul. Power **23**, 44 (2007).
[19] J. L. Rovey, Ph.D. thesis, University of Michigan (2006).
[20] I. H. Hutchinson, *Principles of Plasma Diagnostics*, 2nd ed. (Cambridge University Press, Cambridge, 2002).
[21] R. R. Hofer, Ph.D. thesis, University of Michigan (2004).
[22] Y. Azziz, M. Martinez-Sanchez, and J. Szabo, *Effect of Discharge Voltage on Plume Divergence of a High Specific-Impulse Hall Thruster* (American Institute of Aeronautics and Astronautics, Tucson, AZ, 2005), AIAA-2005-4403.
[23] B. E. Beal, Ph.D. thesis, University of Michigan (2004).
[24] C. H. Reinsche, Numer. Math. **10**, 177 (1967).
[25] D. A. Herman, Ph.D. thesis, University of Michigan (2005).
[26] A. D. Gallimore, J. L. Rovey, and D. A. Herman, "Erosion processes of the discharge cathode assembly of ring-cusp gridded ion thrusters," J. Propul. Power (submitted).
[27] O. B. Duchemin, J. R. Brophy, C. E. Garner, P. K. Ray, V. Shutthanandan, and M. A. Mantenieks, in *Proceedings, 25th International Electric Propulsion Conference* (Electric Rocket Propulsion Society, Cleveland, OH, 1997), IEPC-97-068.
[28] M. R. Nakles, M.S. thesis, Virginia Polytechnic Institute and State University (2004).
[29] Y. Yamamura, Nucl. Instrum. Methods Phys. Res. B **2**, 627 (1984).
[30] R. V. Stuart and G. K. Wehner, J. Appl. Phys. **33**, 1842 (1962).
[31] O. B. Duchemin, Ph.D. thesis, California Institute of Technology (2001).
[32] G. J. Williams, Ph.D. thesis, University of Michigan (2000).
[33] H. E. Wilhelm, Aust. J. Phys. **38**, 125 (1985).
[34] R. P. Doerner, D. G. Whyte, and D. M. Goebel, J. Appl. Phys. **93**, 5816 (2003).